JACS
JOURNAL OF THE AMERICAN CHEMICAL SOCIETY
Communication
pubs.acs.org/JACS

Quantitative Imaging of Ion Transport through Single Nanopores by High-Resolution Scanning Electrochemical Microscopy

Mei Shen, Ryoichi Ishimatsu,† Jiyeon Kim, and Shigeru Amemiya*

Department of Chemistry, University of Pittsburgh, Pittsburgh, Pennsylvania 15260, United States

Supporting Information

ABSTRACT: Here we report on the unprecedentedly high resolution imaging of ion transport through single nanopores by scanning electrochemical microscopy (SECM). The quantitative SECM image of single nanopores allows for the determination of their structural properties, including their density, shape, and size, which are essential for understanding the permeability of the entire nanoporous membrane. Nanoscale spatial resolution was achieved by scanning a 17 nm radius pipet tip at a distance as low as 1.3 nm from a highly porous nanocrystalline silicon membrane in order to obtain the peak current response controlled by the nanopore-mediated diffusional transport of tetrabutylammonium ions to the nanopipet-supported liquid−liquid interface. A 280 nm × 500 nm image resolved 13 nanopores, which corresponds to a high density of 93 nanopores/μm^2. A finite element simulation of the SECM image was performed to assess quantitatively the spatial resolution limited by the tip diameter in resolving two adjacent pores and to determine the actual size of a nanopore, which was approximated as an elliptical cylinder with a depth of 30 nm and major and minor axes of 53 and 41 nm, respectively. These structural parameters were consistent with those determined by transmission electron microscopy, thereby confirming the reliability of quantitative SECM imaging at the nanoscale level.

The development and application of nanoporous membranes for nanofiltration,[1] biomedical devices,[2] nanofluidics,[3] and biomimetic membrane transport[4] require a quantitative understanding of membrane permeability at a single-nanopore level. In fact, it has been theoretically and experimentally demonstrated that the permeability of the whole nanoporous membrane depends on the convolution of several structural properties of nanopores, including their density, shape, and size.[5] Here we applied scanning electrochemical microscopy (SECM)[6] to obtain quantitative and separate determinations of these key structural parameters from high-resolution images of ion transport through single nanopores. Remarkably, the spatial resolution of SECM achieved in this study is the highest reported to date, with the exception of one study,[7] where no quantitative image analysis was shown.

The unprecedentedly high spatial resolution of SECM is required for the imaging of a highly porous nanocrystalline silicon (pnc-Si) membrane[8] at the single-nanopore level. This emerging class of ultrathin nanoporous membranes, with a thickness of 30 nm, are robust enough to be self-standing in aqueous solution and have been found to be useful for unique practical applications that require their high permeability, such as for the efficient separation of macromolecules[8a−c] and nanoparticles,[8d] tissue engineering, and cell culture.[8e] Single-pore imaging, however, has not been reported for a pnc-Si membrane, which not only possesses small nanopores but also has a high pore density with short pore−pore separations of <100 nm. Indeed, its density of ~10^2 pores/μm^2 (Figure 1A) is

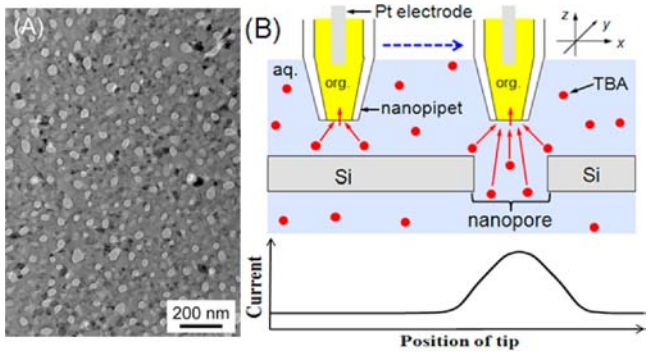

Figure 1. (A) TEM image of a pnc-Si membrane and (B) scheme illustrating an SECM line scan with a nanopipet-supported ITIES tip over the impermeable and nanoporous regions of the membrane.

10^2−10^6 times higher than that of the nanopore membranes (mainly track-etched polymer membranes) that were used for the electrochemical imaging of single pores by SECM,[9] scanning ion-conductance microscopy (SICM),[10] SECM−SICM,[11] and SECM−atomic force microscopy (AFM).[12] In these previous imaging studies, the shortest separations between two resolvable pores were limited to >250 nm and ~1.5 μm for SECM(−AFM)[12b] and SICM,[10f] respectively. On the other hand, micrometer-sized SECM tips were used to probe the local permeability of a pnc-Si membrane based on several thousands of nanopores.[5b,c]

In this work, nanoscale spatial resolution of a pnc-Si membrane was achieved by scanning a small SECM tip with a radius of 17 nm at exceptionally short distances as low as 1.3 nm. Specifically, the current response at the nanotip is based on diffusion-controlled ion transfer at the interface between two immiscible electrolyte solutions (ITIES), which is supported at the tip of the quartz nanopipet filled with an organic electrolyte

Received: March 10, 2012
Published: June 1, 2012

   dx.doi.org/10.1021/ja3023785 | J. Am. Chem. Soc. 2012, 134, 9856−9859

solution[13] (Figure 1B). The ionic tip current is suppressed when the tip is positioned within a tip diameter from the impermeable region of a pnc-Si membrane, which hinders ion diffusion to the nanoscale ITIES tip (i.e., negative feedback effect).[6] In contrast, the tip current increases as the tip is laterally scanned over a nanopore, which mediates ion diffusion to the ITIES tip. Subsequently, a peak-shaped response is obtained during a line scan over a pore (Figure 1B), where a shorter tip−membrane distance enhances the image contrast based on the peak height and improves the spatial resolution based on the peak width.[6]

A nanopipet-based SECM tip was prepared as reported elsewhere[13b] and characterized by ion-transfer voltammetry and scanning electron microscopy (SEM). A nanopipet was filled with a 1,2-dichloroethane solution of organic supporting electrolytes and immersed in an aqueous solution of tetrabutylammonium (TBA) to drive TBA transfer voltammetrically across the nanopipet-supported ITIES tip (Figure 2A). The sigmoidal steady-state voltammograms on the forward

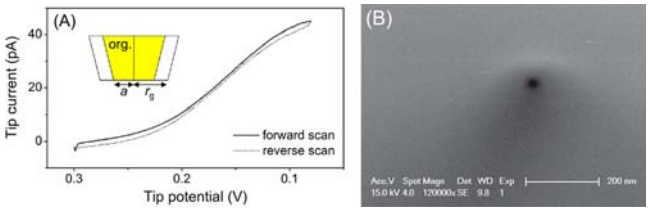

Figure 2. (A) Cyclic voltammetry of 10 mM TBA in 0.3 M KCl at 50 mV/s. The tip potential was defined relative to a Ag/AgCl reference electrode. (B) SEM image of the tip opening of a typical nanopipet.

and reverse potential sweeps showed small capacitive current and nearly overlapped with each other. The pipet-supported ITIES tip was assumed to be an inlaid disk, for which a limiting current, $i_{T,\infty}$, of 42 pA corresponds to a tip inner radius, a, of 17 nm with a typical tip outer radius, r_g, of 1.4a, as determined from the expression

$$i_{T,\infty} = 4xnFDc^*a \quad (1)$$

where x is a function of the quantity $RG = r_g/a$,[16] $n = +1$ is the number of transferred charges in the tip reaction, and $D = 5.1 \times 10^{-6}$ cm^2/s and $c^* = 10$ mM are the diffusion coefficient and concentration of the transferred ion in the bulk solution, respectively. The inner radius of the ITIES tip was similar to that of a typical nanopipet (~15 nm) as estimated by SEM (Figure 2B).

The nanopipet-supported ITIES tip was employed for the imaging of a pnc-Si membrane using SECM in constant-height mode[6] (i.e., without the active feedback control of the tip−membrane distance) in a newly developed isothermal chamber that suppresses distance changes due to thermal drift to a subnanometer level.[13b] In addition, the flat surface of the pnc-Si membrane, with a root-mean-square roughness of 0.29 nm as measured by AFM,[14] was horizontally aligned on the SECM stage using a bubble level[15] to be perpendicular to the tip electrode axis. Subsequently, we observed that a sharp nanopipet with small RG of 1.4 approached very close to the flat substrate and was scanned laterally without contact when a relatively small area of the membrane was imaged [see below; also see Figure S-1 in the Supporting Information (SI) for details].

The whole procedure for obtaining an SECM image (Figure 3A) is illustrated in Figure 3B using the corresponding time

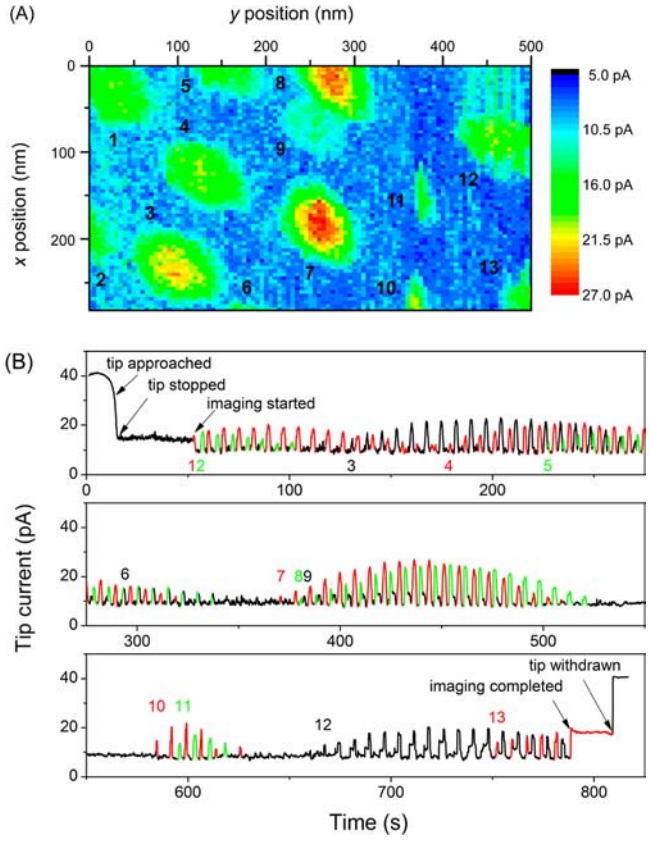

Figure 3. (A) SECM image of a pnc-Si membrane. (B) Tip current vs time profile during the whole imaging experiment. A number is given for each pore at the time when its first peak appears.

profile of the current response at the nanopipet-supported ITIES tip. Prior to imaging, the tip was brought in close proximity to a pnc-Si membrane and stopped when the tip current had decreased to 40% of $i_{T,\infty}$ (Figure 3B). In this example, the tip approached the pore labeled as 1 at $(x, y) = (0, 0)$ (Figure 3A). The tip was held over this pore for 35 s and then scanned from $x = 0$ nm to $x = 280$ nm with a step size of 4 nm; the x line scan was repeated from $y = 0$ nm to $y = 500$ nm at intervals of 5 nm. It took ~0.1 s at each tip position to move and settle the (x, y)-axes piezopositioner and monitor the steady-state tip current.

During the 280 nm × 500 nm scan (Figure 3A), the height of the peak current response to a pore under the tip varied with the lateral distance between the tip and the pore, thereby yielding a family of peaks with various heights for each nanopore (Figure 3B). In contrast, the negative feedback current at the foot of a current peak was very stable and reproducible, which confirmed that the tip−membrane distance was nearly constant during imaging. A tip current, i_T, of 10 pA in Figure 3B is equivalent to a tip−membrane distance of 1.3 nm in the approximate equation with $RG = 1.4$.[13b] A stable distance was also maintained between the tip and pore 13 to give a constant current after the imaging was completed. Finally, the tip current nearly recovered to the initial $i_{T,\infty}$ value when the tip was withdrawn to 1.5 μm away from the substrate. The good stability of the tip current indicated a lack of

dx.doi.org/10.1021/ja3023785 | J. Am. Chem. Soc. 2012, 134, 9856−9859

significant tip damage due to tip−membrane contact during imaging.

Overall, 13 pores were successfully resolved as local regions with higher tip currents in the SECM image of a pnc-Si membrane (Figure 3A). This result corresponds to a high density of 93 nanopores/μm^2, which is consistent with the density of ∼90 nanopores/μm^2 determined from the transmission electron microscopy (TEM) image (Figure 1A). Qualitatively, a larger pore occupies a larger area in the SECM image, where pores 9, 10, and 11 are significantly smaller than the other pores. The area occupied by a pore in the image, however, is larger than expected from the actual size of the pore, because the spatial resolution was limited by the tip size, which was comparable to the pore size. Therefore, quantitative analysis of the SECM image was needed to evaluate the pore size reliably (see below). Noticeably, a unidirectional orientation for some pores can be seen in the SECM image, which may be due to the imperfect disk shape of the ITIES tip supported at an elongated tip orifice. We found that the orientation of nanopores varied from tip to tip, but was independent of the tip−membrane distance (1.3−8.5 nm), and was different from the direction of the tip scan (Figure 3A).

SECM line scans over pore 7 were analyzed by employing a finite element simulation of ion diffusion around the tip and the nanopore (see the SI) to obtain a reliable determination of the actual pore size without the limitation of spatial resolution set by the tip size (Figure 4). For simplicity, the (x, y) cross section

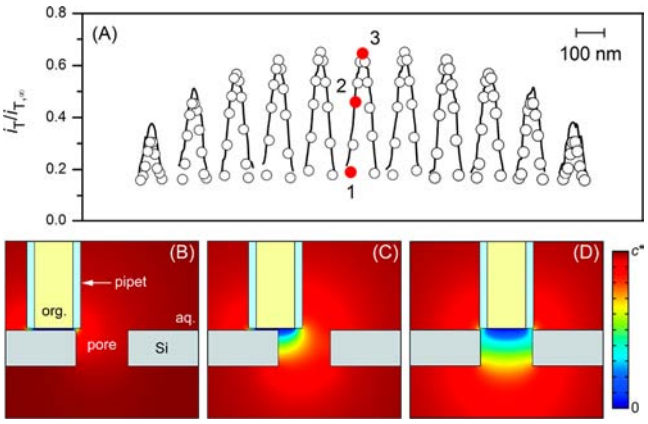

Figure 4. (A) Simulated (circles) and experimental (solid lines) normalized tip currents $i_T/i_{T,\infty}$ for x line scans over pore 7. In the simulation, the y positions of the tip center were kept at Δy = −35, −25, −15, −10, −5, 0, +5, +10, +15, +25, and +35 nm in going from the leftmost peak to the rightmost peak, while the x positions for each line scan were Δx = −42.5, −34, −25.5, −17, −8.5, 0, +8.5, +17, +25.5, +34, and +42.5 nm in going from the leftmost circle to the rightmost circle. Sliced concentration profiles are shown for tip positions with Δy = 0 nm and Δx = (B) −42.5, (C) −25.5, and (D) 0 nm, as indicated by the red dots labeled 1−3, respectively, in part (A).

of a pore was assumed to be elliptical in shape, thereby yielding the major and minor axes and the depth of the pore as structural parameters. TBA is small enough to diffuse freely through a nanopore without electrostatic or steric hindrance from the pore wall.[5c] Very good fits of the simulation results with the experimental results are shown in Figure 4A, where the peak current response in an x line scan was plotted against Δx, the x position of the center of the tip with respect to that of the center of each nanopore, for various values of Δy, which represents the corresponding relative y position of the tip (also see Figure S-3 for these definitions). The simulation results showed that pore 7 has major and minor axes of 53 and 41 nm, respectively. This aspect ratio of 1.3 is consistent with the corresponding values of 1.0−2.1 determined from ∼150 pores in the TEM image (Figure 1A). Moreover, the average of the major and minor axes gave an apparent pore diameter[5b] of 47 nm, which is in agreement with the corresponding values of 14−58 nm in the TEM image. Moreover, the apparent diameter determined by numerical simulation was much smaller than the apparent pore diameter of ∼80 nm for pore 7 determined from its SECM image, where major and minor axes of ∼90 and ∼70 nm, respectively, were obtained from the area surrounded by a contour line of ∼11 pA. Noticeably, a pore depth of 30 nm was also confirmed by the simulation of the peak currents in Figure 4A, which are sensitive to the pore depth (see Figure S-4).

The simulated concentration profiles of TBA around pore 7 during the x line scan at Δy = 0 nm (Figure 4B−D) quantitatively demonstrate how the tip size limits the spatial resolution in determining the actual pore size and separation between two adjacent nanopores. In Figure 4B, the center of the tip was positioned approximately one tip radius away from the edge of the pore, and thus, the whole tip surface was positioned above the impermeable region of the membrane. The resultant negative feedback current determined the base of the current peak (red dot 1 in Figure 4A). Therefore, the apparent pore size estimated from the current peak (or the SECM image) is larger than the actual pore size by a tip inner diameter of 34 nm, which was confirmed for pore 7 with apparent diameters of ∼80 and 47 nm as determined from the SECM image and its simulation, respectively (see above). In fact, when the center of the tip was positioned above the edge of the nanopore (Figure 4C), the corresponding tip current (red dot 2) was significantly enhanced by ion diffusion from the inside of the pore and had already reached more than half of the peak current (red dot 3), which was obtained when the tip center was positioned above the center of the nanopore (Figure 4D). These results also indicate that two adjacent nanopores can be completely separated in the SECM image only when their edge−edge separation is larger than the tip inner diameter. For instance, pore 8 partially overlaps with pore 9 in Figure 3A because their center−center separation of only ∼55 nm is comparable to a typical pore diameter.

In summary, SECM was successfully used to generate unprecedentedly high resolution and quantitative imaging of single nanopores at a high density of 93 nanopores/μm^2. The SECM image could be analyzed quantitatively to determine the structural properties of single nanopores, including the smallest pore axis of 41 nm, without the limitation of spatial resolution set by the tip diameter. The numerical simulation also indicated that two adjacent pores with an edge−edge separation equal to or larger than the tip diameter (i.e., ≥34 nm in this work) would be completely resolvable. Advantageously, the highest resolution of SECM under normal experimental conditions was achieved in this study by employing the simple constant-height mode without feedback distance control, not only because the pnc-Si membrane surface was flat, but also because the SECM stage was isolated from the ambient environment using an isothermal chamber to suppress thermal drift.[13b] On the basis of these findings, we envision the application of this simple, quantitative, and high-resolution SECM approach to the imaging of biological nanopores.[17]

dx.doi.org/10.1021/ja3023785 | J. Am. Chem. Soc. 2012, 134, 9856−9859

■ ASSOCIATED CONTENT

Supporting Information

Experimental methods, simulation details, and additional results. This material is available free of charge via the Internet at http://pubs.acs.org.

■ AUTHOR INFORMATION

Corresponding Author

amemiya@pitt.edu

Present Address

[†]Department of Applied Chemistry, Graduate School of Engineering, Kyushu University, Nishi-Ku, Fukuoka 819−0395, Japan (R.I.).

Notes

The authors declare no competing financial interest.

■ ACKNOWLEDGMENTS

This work was supported by the National Institutes of Health (GM073439). We thank Dr. Christopher C. Striemer and Mr. Charles Chan, SiMPore, for the TEM images of pnc-Si membranes and their analysis.

■ REFERENCES

(1) (a) Vandezande, P.; Gevers, L. E. M.; Vankelecom, I. F. J. *Chem. Soc. Rev.* **2008**, *37*, 365. (b) Shannon, M. A.; Bohn, P. W.; Elimelech, M.; Georgiadis, J. G.; Marinas, B. J.; Mayes, A. M. *Nature* **2008**, *452*, 301. (c) Peng, X. S.; Jin, J.; Nakamura, Y.; Ohno, T.; Ichinose, I. *Nat. Nanotechnol.* **2009**, *4*, 353. (d) Karan, S.; Samitsu, S.; Peng, X.; Kurashima, K.; Ichinose, I. *Science* **2012**, *335*, 444.

(2) (a) Kooman, J. P.; van der Sande, F. M.; Leunissen, K. M. L. *Blood Purif.* **2007**, *25*, 377. (b) Fissell, W. H.; Dubnisheva, A.; Eldridge, A. N.; Fleischman, A. J.; Zydney, A. L.; Roy, S. *J. Membr. Sci.* **2009**, *326*, 58. (c) Perin, L.; Da Sacco, S.; De Filippo, R. E. *Adv. Drug Delivery Rev.* **2011**, *63*, 379.

(3) (a) van den Berg, A.; Wessling, M. *Nature* **2007**, *445*, 726. (b) Schoch, R. B.; Han, J. Y.; Renaud, P. *Rev. Mod. Phys.* **2008**, *80*, 839. (c) Li, Y.-Q.; Zheng, Y.-B.; Zare, R. N. *ACS Nano* **2012**, *6*, 993.

(4) (a) Jovanovic-Talisman, T.; Tetenbaum-Novatt, J.; McKenney, A. S.; Zilman, A.; Peters, R.; Rout, M. P.; Chait, B. T. *Nature* **2009**, *457*, 1023. (b) Kowalczyk, S. W.; Kapinos, L.; Blosser, T. R.; Magalhaes, T.; van Nies, P.; Lim, R. Y. H.; Dekker, C. *Nat. Nanotechnol.* **2011**, *6*, 433.

(5) (a) Berg, H. C. *Random Walks in Biology*; Princeton University Press: Princeton, NJ, 1993. (b) Kim, E.; Xiong, H.; Striemer, C. C.; Fang, D. Z.; Fauchet, P. M.; McGrath, J. L.; Amemiya, S. *J. Am. Chem. Soc.* **2008**, *130*, 4230. (c) Ishimatsu, R.; Kim, J.; Jing, P.; Striemer, C. C.; Fang, D. Z.; Fauchet, P. M.; McGrath, J. L.; Amemiya, S. *Anal. Chem.* **2010**, *82*, 7127.

(6) (a) *Scanning Electrochemical Microscopy*; Bard, A. J., Mirkin, M. V., Eds.; Marcel Dekker: New York, 2001. (b) Amemiya, S.; Bard, A. J.; Fan, F.-R. F.; Mirkin, M. V.; Unwin, P. R. *Annu. Rev. Anal. Chem.* **2008**, *1*, 95.

(7) Fan, F.-R. F.; Bard, A. J. *Proc. Natl. Acad. Sci. U.S.A.* **1999**, *96*, 14222.

(8) (a) Striemer, C. C.; Gaborski, T. R.; McGrath, J. L.; Fauchet, P. M. *Nature* **2007**, *445*, 749. (b) Fang, D. Z.; Striemer, C. C.; Gaborski, T. R.; McGrath, J. L.; Fauchet, P. M. *Nano Lett.* **2010**, *10*, 3904. (c) Snyder, J. L.; Clark, A.; Fang, D. Z.; Gaborski, T. R.; Striemer, C. C.; Fauchet, P. M.; McGrath, J. L. *J. Membr. Sci.* **2011**, *369*, 119. (d) Gaborski, T. R.; Snyder, J. L.; Striemer, C. C.; Fang, D. Z.; Hoffman, M.; Fauchet, P. M.; McGrath, J. L. *ACS Nano* **2010**, *4*, 6973. (e) Agrawal, A. A.; Nehilla, B. J.; Reisig, K. V.; Gaborski, T. R.; Fang, D. Z.; Striemer, C. C.; Fauchet, P. M.; McGrath, J. L. *Biomaterials* **2010**, *31*, 5408.

(9) (a) Bath, B. D.; White, H. S.; Scott, E. R. In *Scanning Electrochemical Microscopy*; Bard, A. J., Mirkin, M. V., Eds.; Marcel Dekker: New York, 2001; p 343. (b) Uitto, O. D.; White, H. S. *Anal. Chem.* **2001**, *73*, 533. (c) Uitto, O. D.; White, H. S.; Aoki, K. *Anal. Chem.* **2002**, *74*, 4577. (d) Lee, S.; Zhang, Y.; White, H. S.; Harrell, C. C.; Martin, C. R. *Anal. Chem.* **2004**, *76*, 6108. (e) Ervin, E. N.; White, H. S.; Baker, L. A. *Anal. Chem.* **2005**, *77*, 5564. (f) Ervin, E. N.; White, H. S.; Baker, L. A.; Martin, C. R. *Anal. Chem.* **2006**, *78*, 6535. (g) White, R. J.; White, H. S. *Anal. Chem.* **2007**, *79*, 6334. (h) McKelvey, K.; Snowden, M. E.; Peruffo, M.; Unwin, P. R. *Anal. Chem.* **2011**, *83*, 6447.

(10) (a) Proksch, R.; Lal, R.; Hansma, P. K.; Morse, D.; Stucky, G. *Biophys. J.* **1996**, *71*, 2155. (b) Böcker, M.; Muschter, S.; Schmitt, E. K.; Steinem, C.; Schäffer, T. E. *Langmuir* **2009**, *25*, 3022. (c) Chen, C.-C.; Derylo, M. A.; Baker, L. A. *Anal. Chem.* **2009**, *81*, 4742. (d) Chen, C.-C.; Baker, L. A. *Analyst* **2011**, 136. (e) Chen, C.-C.; Zhou, Y.; Baker, L. A. *ACS Nano* **2011**, *5*, 8404. (f) Zhou, Y.; Chen, C.-C.; Baker, L. A. *Anal. Chem.* **2012**, *84*, 3003.

(11) (a) Takahashi, Y.; Shevchuk, A. I.; Novak, P.; Zhang, Y.; Ebejer, N.; Macpherson, J. V.; Unwin, P. R.; Pollard, A. J.; Roy, D.; Clifford, C. A.; Shiku, H.; Matsue, T.; Klenerman, D.; Korchev, Y. E. *Angew. Chem., Int. Ed.* **2011**, *50*, 9638. (b) Morris, C. A.; Chen, C.-C.; Baker, L. A. *Analyst* **2012**, DOI: 10.1039/C2AN16178H.

(12) (a) Macpherson, J. V.; Unwin, P. R. *Anal. Chem.* **2000**, *72*, 276. (b) Macpherson, J. V.; Jones, C. E.; Barker, A. L.; Unwin, P. R. *Anal. Chem.* **2002**, *74*, 1841. (c) Gardner, C. E.; Unwin, P. R.; Macpherson, J. V. *Electrochem. Commun.* **2005**, *7*, 612.

(13) (a) Elsamadisi, P.; Wang, Y.; Velmurugan, J.; Mirkin, M. V. *Anal. Chem.* **2011**, *83*, 671. (b) Kim, J.; Shen, M.; Nioradze, N.; Amemiya, S. *Anal. Chem.* **2012**, *84*, 3489.

(14) Fang, D. Z. Ph.D. Dissertation, University of Rochester, Rochester, NY, 2010.

(15) Sun, P.; Mirkin, M. V. *Anal. Chem.* **2006**, *78*, 6526.

(16) Lefrou, C. *J. Electroanal. Chem.* **2006**, *592*, 103.

(17) Guo, J.; Amemiya, S. *Anal. Chem.* **2005**, *77*, 2147.